

---

# Environmental Concentrations of PFOS Selectively Accumulate in the *Euglena* Eyespot and Directly Inhibit Chloroplast ATP Synthase: A Dual Impairment of Phototaxis and Photosynthetic Light Reactions Without Inhibiting Photosynthesis

---

[Peirui Liu](#)\*, [Junfeng Wang](#), Yan Hong, Zilin Chen, Xiaoya Liu, [Huayi Chen](#), [Ganning Zeng](#), [Xiangliang Pan](#)

Posted Date: 22 April 2026

doi: 10.20944/preprints202604.1506.v1

Keywords: *Euglena gracilis*; PFOS; eyespot; phototaxis; ATP synthase; photophosphorylation; dual impairment



Preprints.org is a free multidisciplinary platform providing preprint service that is dedicated to making early versions of research outputs permanently available and citable. Preprints posted at Preprints.org appear in Web of Science, Crossref, Google Scholar, Scilit, Europe PMC.

Copyright: This open access article is published under a [Creative Commons CC BY 4.0 license](#), which permit the free download, distribution, and reuse, provided that the author and preprint are cited in any reuse.

Disclaimer/Publisher's Note: The statements, opinions, and data contained in all publications are solely those of the individual author(s) and contributor(s) and not of MDPI and/or the editor(s). MDPI and/or the editor(s) disclaim responsibility for any injury to people or property resulting from any ideas, methods, instructions, or products referred to in the content.

Article

# Environmental Concentrations of PFOS Selectively Accumulate in the *Euglena* Eyespot and Directly Inhibit Chloroplast ATP Synthase: A Dual Impairment of Phototaxis and Photosynthetic Light Reactions Without Inhibiting Photosynthesis

Peirui Liu <sup>1,\*</sup>, Junfeng Wang <sup>1</sup>, Yan Hong <sup>1</sup>, Zilin Chen <sup>1</sup>, Xiaoya Liu <sup>2</sup>, Huayi Chen <sup>3</sup>, Ganning Zeng <sup>1</sup> and Xiangliang Pan <sup>1</sup>

<sup>1</sup> Zhejiang Key Laboratory of Low-carbon Control Technology for Industrial Pollution, College of Environment, Zhejiang University of Technology, Hangzhou 310014, China

<sup>2</sup> School of Environmental Science and Engineering, Xiamen University of Technology, Xiamen 361024, China

<sup>3</sup> School of Tropical Agriculture and Forestry, Hainan University, Haikou, 570228, China

\* Correspondence: liupeirui1013@zjut.edu.cn

## Abstract

Perfluorooctane sulfonate (PFOS) is a persistent organic pollutant widely detected in aquatic ecosystems, but its subcellular targets and the mechanisms by which it disrupts light resource utilization in photosynthetic protozoa remain poorly understood at environmentally relevant concentrations. Here, *Euglena gracilis* was exposed to environmentally relevant PFOS concentrations. Subcellular distribution, phototaxis, photosynthetic light reactions, and energy metabolism were investigated using isolated chloroplast assays, transcriptomics, and proteomics. PFOS accumulated prominently in the eyespot and chloroplasts. Eyespot accumulation impaired phototactic motility and increased the light perception threshold. PFOS did not acutely inhibit overall photosynthesis; instead, a transient upregulation of photosynthesis-related genes and a slight stimulation of oxygen evolution were observed, which weakened with prolonged exposure. PFOS significantly reduced ATP levels and the photosynthetic electron transport rate (*ETR*), while *Fv/Fm* remained unchanged and non-photochemical quenching (*NPQ*) was elevated. Isolated chloroplast assays confirmed direct inhibition of Mg<sup>2+</sup>-ATP synthase and thylakoid electron transport. Transcriptomic and proteomic analyses revealed compensatory upregulation of photosynthesis pathways but suppression of ATP synthesis and redox homeostasis. Mechanistically, PFOS directly targets chloroplast ATP synthase, leading to proton gradient accumulation, feedback inhibition of electron transport, and increased *NPQ*. Together with eyespot-mediated phototaxis impairment, PFOS dually disrupts light acquisition (behavioral) and light conversion (physiological). This dual impairment may compromise the ecological fitness of *Euglena* in PFOS-contaminated environments, especially under prolonged exposure.

**Keywords:** *Euglena gracilis*; PFOS; eyespot; phototaxis; ATP synthase; photophosphorylation; dual impairment

## 1. Introduction

Perfluorooctane sulfonate (PFOS), a representative persistent organic pollutant of per- and polyfluoroalkyl substances (PFAS), is widely detected in surface waters at concentrations typically below 300 ng/L, but can exceed this level in contaminated hotspots [1–8]. Unlike classical lipophilic pollutants, PFOS exhibits surfactant properties and a strong affinity for proteins, preferentially

binding to fatty acid-binding proteins and albumin[9]. This protein-binding behavior suggests that PFOS may selectively accumulate in protein-rich subcellular structures.

*Euglena gracilis* is a unicellular eukaryote capable of both photosynthetic autotrophy and heterotrophy. At the anterior end of the cell, *Euglena* possesses a stigma (eyespot) composed of a lipoprotein complex rich in carotenoids and rhodopsin-like proteins, which senses light intensity and direction and modulates flagellar movement to drive phototaxis[10,11]. The photoactivated adenylyl cyclase (PAC) within the eyespot is a core phototransduction protein; upon blue-light stimulation, PAC promotes cAMP production, thereby regulating flagellar motility[12]. Phototactic behavior determines the spatial positioning of cells in a light environment and thus influences the efficiency of light resource acquisition in *Euglena*.

Preliminary observations using transmission electron microscopy combined with energy-dispersive X-ray spectroscopy mapping (TEM-EDS mapping) revealed that after PFOS exposure, fluorine signal intensity was notably enhanced in the eyespot region, indicating local enrichment. Most existing studies on the effects of PFOS on photosynthetic organisms have focused on direct chloroplast damage under relatively high concentrations[13], whereas little attention has been paid to whether the eyespot, a photoreceptive structure, is also affected. Moreover, direct molecular evidence for an interaction between PFOS and the eyespot photoreceptor PAC remains lacking. Given the eyespot's critical role in light perception and energy acquisition, understanding whether PFOS targets this organelle at environmentally relevant concentrations is essential for assessing its ecological risks to photosynthetic flagellates

The present study therefore addresses the following questions: (i) Does environmentally relevant PFOS accumulate in the *Euglena* eyespot and concurrently induce phototactic abnormalities? (ii) Does PFOS directly affect chloroplast energy conversion? (iii) What is the relationship between eyespot-mediated behavioral impairment and photosynthetic physiological changes? To address these questions, we examined the subcellular distribution of PFOS using TEM-EDS mapping, analyzed its potential interaction with PAC via molecular docking, and assessed eyespot function through phototactic motility, flagellar shedding rate, and swimming speed. Photosynthetic and metabolic status were evaluated by measuring chlorophyll fluorescence parameters (including  $F_v/F_m$ ,  $ETR$ ,  $NPQ$ ), chlorophyll content, intracellular ATP and ROS levels. Isolated chloroplast assays were performed to distinguish direct from indirect effects, and transcriptomic and proteomic analyses were used to characterize molecular response signatures.

## 2. Materials and Methods

### 2.1. Cultivation of *Euglena Gracilis* and PFOS Exposure

*Euglena gracilis* (*E. gracilis*) strain FACHB-848 was obtained from the Institute of Hydrobiology, Chinese Academy of Sciences. Stock cultures were maintained in sterile EM medium under controlled conditions: a 12 h:12 h light-dark cycle with cool-white fluorescent illumination (light intensity of 3500 lux) at a temperature of  $25 \pm 1$  °C. Cultures were incubated under the aforementioned light and temperature regime until they reached the logarithmic growth phase, and the initial optical density at 680 nm ( $OD_{680}$ ) of the culture was adjusted to 0.1 using a UV-visible spectrophotometer (UV1800, Shimadzu Instruments Co., Ltd., Japan). The relationship between  $OD_{680}$  and cell density was determined by a standard curve: cell density ( $\times 10^4$  cells/mL) =  $65.042 \times OD_{680} + 1.5846$  ( $R^2 = 0.9996$ ). Subsequently, a stock solution of PFOS was added to achieve final exposure concentrations of 0.0, 0.5, 5.0, and 50.0  $\mu\text{g/L}$ . All subsequent experiments were performed using cells derived from at least three independent culture batches for each trophic condition to ensure biological reproducibility.

#### 2.1.1. PFOS Quantification

PFOS concentrations were quantified using ultra-performance liquid chromatography (UPLC, ACQUITY UPLC I-Class, Milford, MA, USA) coupled with tandem mass spectrometry (XEVO TQ-S,

Waters, Milford, MA, USA). The system was equipped with an ACQUITY UPLC BEH C18 column (2.1 mm × 100 mm, particle size 1.7 μm, Waters, Milford, MA, USA) and an electrospray ionization (ESI) source. The mobile phase consisted of 5 mmol/L ammonium acetate (solution A) and 100% methanol (solution B). Samples were directly injected into the UPLC system and eluted at a flow rate of 0.2 mL/min. Mass spectrometry was performed in negative ESI mode with optimized conditions as follows: drying gas (N<sub>2</sub>) temperature 300 °C, drying gas flow 6 L/min, sheath gas (N<sub>2</sub>) temperature 260 °C, sheath gas flow 11 L/min[14]. LC-MS data were acquired in multiple reaction monitoring (MRM) mode and processed using MassLynx 4.1 software. A standard curve was constructed using PFOS standard solutions at concentrations of 1.0, 5.0, 10.0, 50.0, and 200.0 μg/L, yielding an R<sup>2</sup> of 0.9995. Prior to use, PFOS was further calibrated by gas chromatography-tandem mass spectrometry (GC-MS/MS). All glassware used in the experiment was sequentially washed with methanol and ultrapure water, then ultrasonicated, dried, wrapped in aluminum foil, and baked in a muffle furnace at 350 °C for 4 h.

### 2.1.2. Visualization of PFOS Accumulation in the Eyespot

*E. gracilis* cells were fixed in 2.5% (v/v) glutaraldehyde for two days. The cells were then suspended in 2.5% warm agar. After solidification, small cubes were cut from the sample and post-fixed in 1% (w/v) OsO<sub>4</sub> for 1 h. The fixatives were buffered with 0.07 M Na<sub>2</sub>HPO<sub>4</sub>-KH<sub>2</sub>PO<sub>4</sub> (pH 7.2). Following dehydration in a graded ethanol series, the samples were embedded in Durcupan ACM resin. Ultrathin sections were cut using a Reichert Jung Ultracut M microtome (Reichert-Jung Ltd., Austria), mounted on copper grids, stained with 5% uranyl acetate and Reynold's lead citrate solution, and observed under a transmission electron microscope (TEM)[15].

### 2.1.3. Molecular Docking Analysis

To predict the binding mode between PFOS and the photoreceptor protein photoactivated adenylyl cyclase (PAC) in the *Euglena* eyespot, the amino acid sequence of PAC was retrieved from the UniProt database. As no crystal structure of PAC is currently available, a dimeric model was generated using ProteinX and subsequently energy-minimized with Rosetta Relax. The obtained three-dimensional (3D) protein structure was preprocessed using PyMOL software by removing water molecules and adding hydrogen atoms, and the final structure was saved in PDB format. The SMILES string of PFOS was obtained from the PubChem database, and its 3D structure was optimized using Python with the RDKit toolkit based on the MMFF94 force field. Molecular docking was performed using CB-DOCK2 software for blind docking[16]. CB-DOCK2 employs an artificial neural network for cavity detection and uses AutoDock Vina to perform the docking calculations. The optimal protein-ligand complex was selected based on the predicted binding energy (calculated with the AMBER force field), followed by analysis of intermolecular interactions and evaluation of the docking pose. Non-covalent interactions between the ligand and receptor were analyzed using PLIP software, and the 3D conformational diagrams were visualized with PyMOL.

## 2.2. Phototactic Behavior Assays

### 2.2.1. Determination of Vertical and Horizontal Swimming Speed

A laboratory microscale device was used to measure the swimming ability of *E. gracilis* (Figure 1). For vertical movement experiments, a cylindrical acrylic channel with an inner diameter of 4.4 cm and a height of 10.0 cm was employed. The channel was illuminated from above by a white/blue LED lamp (3500 lux) for 20 min, and sampling points were set every 3.0 cm[17]. For horizontal movement experiments, a rectangular acrylic channel with a square cross-section (inner width 4.0 cm, length 9.0 cm) was used. Illumination was provided from the side by a white/blue LED lamp (3500 lux) for 20 min, with sampling points every 3.0 cm. Only the side facing the light source was transparent. The swimming speed was calculated using the following formula:

$$Velocity = (C_1V_1 \times S_1 + C_2V_2 \times S_2 + \dots + C_{10}V_{10} \times S_{10}) / t \quad (C_1V_1 + C_2V_2 + \dots + C_{10}V_{10})$$

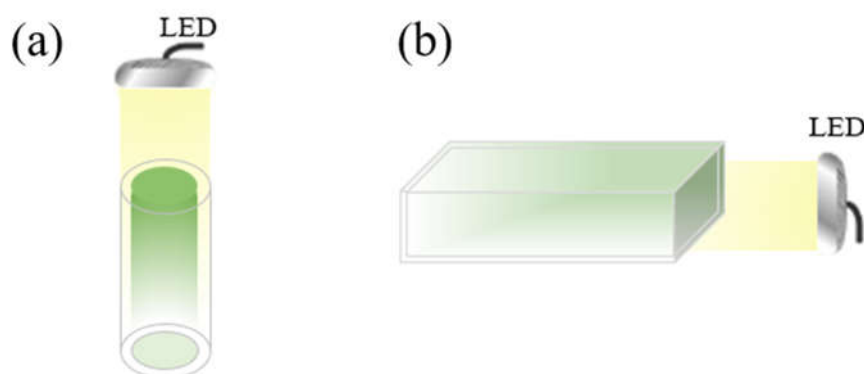


**Figure 1.** The schematic diagram of the swimming device. (a) vertical movement; (b) horizontal movement.

### 2.2.2. Phototactic Movement Assay

For phototaxis experiments, the rectangular acrylic channel described above (Figure 1a) was used. *E. gracilis* cells exposed to PFOS under autotrophic conditions were placed at the end of the channel near the light source. The channel was illuminated from the side by a white/blue LED lamp for 20.0 min, with light intensity increasing stepwise from 2000 lux to 10,000 lux in increments of 2000 lux. Subsequently, samples were collected from both the near-light end and the far-light end, and the ratio of cell density at the near-light end to that at the far-light end was calculated.

### 2.2.3. Determination of Flagellar Shedding Rate

The flagellar shedding of *E. gracilis* cells was observed under a microscope, and the flagellar shedding rate was calculated. An aliquot of 20.0  $\mu\text{L}$  of algal suspension was placed on a hemocytometer and allowed to settle for 5.0 min. A total of 300 cells were randomly counted to determine the flagellar shedding rate. Each sample was measured in triplicate, and three independent parallel experiments were performed.

### 2.3. Growth Curve and Photosynthetic Activity Measurement

*E. gracilis* cells at the logarithmic growth phase were collected and resuspended in freshly prepared culture medium to adjust the optical density at 680 nm ( $\text{OD}_{680}$ ) to 0.1. The cells were then exposed to PFOS at concentrations of 0, 0.5, 5.0, 50.0, and 500.0  $\mu\text{g/L}$ . Samples were taken every 24 h over a period of 10 days to determine cell density. The maximum photochemical quantum yield of photosystem II ( $F_v/F_m$ ) and non-photochemical quenching ( $NPQ$ ) were measured daily using an AquaPen-C AP 110-C pulse-amplitude-modulated fluorometer (Photon Systems Instruments, Czech Republic) after a 15-minute dark adaptation period.

### 2.4. Chlorophyll Extraction and Quantification

Aliquots of 10 mL of cell suspension cultured for 7 days were filtered and rinsed three times with distilled water. The cells were then ground with glass sand and 80% (v/v) acetone solution until the pigments were completely transferred to the solvent. The homogenate was filtered again to remove insoluble residues. The filtrate was collected and brought to a final volume of 10 mL with 80% acetone. The absorbance of the extract was measured at 470, 646, and 663 nm using a UV-Vis spectrophotometer [18]. Photosynthetic pigment concentrations ( $\text{mg}\cdot\text{L}^{-1}$ ) were calculated according to the following equations:

$$C_a = 12.21 \text{Abs}_{663} - 2.81 \text{Abs}_{646}$$

$$C_b = 20.13 \text{Abs}_{646} - 5.03 \text{Abs}_{663}$$

$$C_{x+c} = (1000 \text{Abs}_{470} - 3.27 \text{Chl}_a - 104 \text{Chl}_b) / 229$$

where  $C_a$ ,  $C_b$  and  $C_{x+c}$  are Chlorophyll a ( $\text{Chl}_a$ ), Chlorophyll b ( $\text{Chl}_b$ ), carotenoids and other pigments ( $C_{x+c}$ ), respectively.

### 2.5. Intracellular ATP Level Measurement

Intracellular ATP levels in *E. gracilis* were determined using an ATP Assay Kit (Beyotime Biotechnology, China). After PFOS exposure, cells were collected by centrifugation at 3000 rpm. The cell pellet was resuspended in 200.0  $\mu\text{L}$  of lysis buffer and vortexed. Following lysis, the mixture was centrifuged at  $12,000 \times g$  for 5 min at 4 °C. The supernatant (100.0  $\mu\text{L}$ ) was collected, and the relative luminescence unit (RLU) was measured using a multimode microplate reader.

### 2.6. Intracellular Reactive Oxygen Species (ROS) Level Measurement

Intracellular ROS levels were measured using a Reactive Oxygen Species Assay Kit (Beyotime Biotechnology, China). After PFOS exposure, cells were collected by centrifugation at 3000 rpm. The cell pellet was resuspended in phosphate-buffered saline (PBS) containing 2',7'-dichlorodihydrofluorescein diacetate (DCFH-DA) diluted 1:2000 (v/v) in PBS. The suspension was incubated at 37 °C for 20 min. The cells were then washed three times with serum-free culture medium. Cells treated with the ROS positive control provided in the kit served as the control group. The stained cells were analyzed using a flow cytometer with excitation at 488 nm and emission at 525 nm. A total of 12,000 events were recorded per sample.

### 2.7. Assays of Isolated Chloroplast Function

Chloroplasts were isolated from *E. gracilis* cells cultured under autotrophic conditions for 10 days using a High-Purity Chloroplast Isolation Kit (density gradient method, Beyotime Biotechnology, China), and the isolated chloroplasts were characterized by fluorescence microscopy. The bioaccumulation of organic pollutants in the environment is influenced by multiple factors, including subcellular distribution, the specific surface area of organisms, and environmental concentrations[19,20]. Studies have shown that PFOS concentrations at the subcellular level typically range from pg/g to  $\mu\text{g/g}$ , generally not exceeding 10 ng/g, although levels may exceed this value in tissues or organelles prone to PFOS accumulation[21,22]. Therefore, isolated chloroplasts were exposed to PFOS at concentrations of 0, 5.0, 50.0, and 500.0 ng/L, which are lower than the in vivo exposure concentrations, to verify the direct action potential of PFOS on chloroplasts.

#### 2.7.1. Photophosphorylation Assay

An aliquot of 0.1 mL of chloroplast suspension was mixed with 0.9 mL of reaction buffer containing 0.015 mol/L Tris-HCl, 0.035 mol/L NaCl, 0.01 mmol/L  $\text{MgCl}_2$ , 1  $\mu\text{mol/L}$  ATP, and 1  $\mu\text{mol/L}$   $\text{K}_3\text{Fe}(\text{CN})_6$ . The mixture was illuminated at 3500 lux for 1 min at 25 °C. Inorganic phosphorus content was then determined.

#### 2.7.2. $\text{Mg}^{2+}$ -ATPase Activity Assay

An aliquot of 0.1 mL of chloroplast suspension was mixed with 0.5 mL of activation buffer containing 25 mmol/L Tris-HCl, 50.0 mmol/L NaCl, 5.0 mmol/L  $\text{MgCl}_2$ , 1  $\mu\text{mol/L}$  EDTA, and 200.0  $\mu\text{g}$  trypsin. The mixture was illuminated at 25 °C for 5 min for activation, and the reaction was terminated by adding 0.1 mL of bovine serum albumin (5 mg/mL). Subsequently, 0.5 mL of reaction buffer containing 50.0 mmol/L Tris-HCl, 5.0 mmol/L  $\text{MgCl}_2$ , and 5.0  $\mu\text{mol/L}$  ATP was added. The mixture was incubated in a water bath at 37 °C for 10 min, and the reaction was terminated by adding

0.1 mL of 20% trichloroacetic acid. After centrifugation, the supernatant was collected to determine ATP hydrolysis-derived inorganic phosphorus.

### 2.7.3. Ca<sup>2+</sup>-ATPase Activity Assay

An aliquot of 0.1 mL of chloroplast suspension was mixed with 0.5 mL of activation buffer containing 25 mmol/L Tris-HCl, 2  $\mu$ mol/L EDTA, and 1  $\mu$ mol/L ATP. The mixture was illuminated at 25 °C for 5 min for activation, and the reaction was terminated by adding 0.1 mL of bovine serum albumin (5.0 mg/mL). Subsequently, 0.5 mL of reaction buffer containing 50 mmol/L Tris-HCl, 2 mmol/L CaCl<sub>2</sub>, and 10  $\mu$ mol/L ATP was added. The mixture was incubated in a water bath at 37 °C for 10 min, and the reaction was terminated by adding 0.1 mL of 20% trichloroacetic acid. After centrifugation, the supernatant was collected to determine ATP hydrolysis-derived inorganic phosphorus.

### 2.7.4. Cytochrome b<sub>6</sub>f Complex Activity Assay

Chloroplasts were isolated and suspended in a buffer containing 50 mM K<sub>2</sub>HPO<sub>4</sub> (pH 6.5), 0.33 M sorbitol, 1.0 mM MgCl<sub>2</sub>, 1.0 mM MnCl<sub>2</sub>, 2.0 mM EDTA, and 1% Triton X-100. The chloroplast suspension was exposed to PFOS at concentrations of 0.0, 5.0, 50.0, and 500.0 ng/L, and the absorbance peak at 554 nm was measured[23].

### 2.7.5. Electron Transport Rate Assay

Isolated chloroplasts were resuspended in Tris-HCl buffer and adjusted to a concentration of 50.0–100.0  $\mu$ g chlorophyll/mL. Chlorophyll content was determined using a spectrophotometer at 663 nm and 645 nm, and the concentration was further diluted to the desired range for the experiment. The artificial electron acceptor DCIP (2,6-dichlorophenolindophenol) was freshly prepared at a concentration of 20.0–50.0  $\mu$ M and protected from light to prevent decomposition. Buffer without chloroplasts was added to a cuvette, and the initial absorbance of DCIP at 600 nm was recorded. Chloroplast suspensions containing PFOS at concentrations of 0.0, 5.0, 50.0, and 500.0 ng/L were then mixed with the DCIP solution. The reaction was allowed to proceed under illumination at 5000 lux for 2 min, and the change in absorbance was recorded[24].

### 2.7.6. Cyclic Voltammetry (CV) Measurements

Cyclic voltammetry experiments were conducted in 40.0 mL of solution using a three-electrode system consisting of a glassy carbon working electrode (3.0 mm diameter), a platinum wire counter electrode, and an Ag/AgCl reference electrode. The voltage was scanned from -0.8 V to 1.0 V (vs. Ag/AgCl) at a scan rate of 0.1 V/s.

### 2.7.7. Electrochemical Impedance Spectroscopy (EIS) Measurements

Electrochemical impedance spectroscopy (EIS) was performed to probe the electrical properties of the chloroplast/electrode interface, and was performed under potentiostatic control at the open-circuit potential (OCP) at room temperature. The electrochemical test system operated over a frequency range of 10<sup>5</sup> to 10<sup>-1</sup> Hz. A standard three-electrode system was employed, with a glassy carbon electrode serving as the working electrode, and an Ag/AgCl electrode and a platinum wire as the reference and counter electrodes, respectively. To quantitatively analyze the impedance spectra, the equivalent circuit model shown in Figure S1 was employed. The high-frequency semicircle is attributed to the charge transfer process at the electrode–chloroplast interface, and its diameter corresponds to  $R_2$  (charge transfer resistance), reflecting the efficiency of electron transfer from the photosynthetic electron transport chain to the electrode. The intermediate-frequency semicircle is assigned to the resistance of the thylakoid membrane or the biointerface ( $R_i$ ), which is sensitive to the integrity and ion permeability of the membrane. The low-frequency linear region (with a slope approaching 45°) is characteristic of the Warburg impedance ( $Z_0$ ), indicating that the overall reaction

becomes limited by the diffusion of redox species (e.g., electron carriers or ions) near the electrode surface.

## 2.8. Transcriptomic and Proteomic Analyses

### 2.8.1. Transcriptome Analysis

*E. gracilis* cells exposed to 0.0 or 50.0 µg/L PFOS for 7 days (three biological replicates per group) were harvested for transcriptome analysis. Total RNA was sequenced using the Illumina platform (non-reference approach). Raw reads were filtered to obtain clean reads, which were then de novo assembled into unigenes. The unigenes served as reference sequences for expression quantification, functional annotation, and identification of SNPs and SSRs[25]. Quality control metrics included raw reads (>10 million), raw bases (>100 Mb), clean reads (>70% of raw reads), clean bases (>80 Mb), error rate (<1%), Q20 (≥90%), Q30 (≥85%), and GC content (approximately 62%, within the acceptable range for microalgae[26,27]). All metrics met the standard requirements for reliable transcriptomic analysis.

### 2.8.2. Quantitative Proteome Analysis

Protein extracts from the same samples (0.0 and 50.0 µg/L PFOS, 7 days) were analyzed using data-independent acquisition (DIA) mass spectrometry[28]. A protein database was constructed based on the de novo transcriptome assembly of *E. gracilis*. DIA data were processed for protein identification and quantification. Quality control was assessed by monitoring peptide retention time (RT) consistency across samples and the proportion of unique peptides. Peptides with coefficient of variation (CV) <0.3 and present in all samples were used as internal standards. The majority of identified proteins contained multiple unique peptides, confirming the reliability of the proteomic data[29].

## 2.9. Statistical Analysis

All experiments were conducted with three independent biological replicates, where each replicate originated from a separate algal culture batch. Data are presented as the arithmetic mean ± standard deviation (s.d.). Experimental data were processed using Excel 2022. Graphs were created with Origin 2024. Statistical analyses were performed using IBM SPSS Statistics 27. One-way analysis of variance (ANOVA) followed by Fisher's least significant difference (LSD) post hoc test was used for multiple comparisons. Significant differences among groups are indicated by different lowercase letters (a, b, c, d), with groups sharing the same letter showing no significant difference, and groups with different letters showing significant differences ( $p < 0.05$ ).

## 3. Results and Discussion

### 3.1. Accumulation of PFOS in the Eyespot and Its Effects on Phototaxis and Motility

To investigate the subcellular distribution of PFOS and its relationship with toxic phenotypes, transmission electron microscopy combined with energy-dispersive X-ray spectroscopy mapping (TEM-EDS mapping) was performed on *E. gracilis* cells exposed to 50.0 µg/L PFOS for 7 days. As shown in Figure 1, PFOS accumulation exhibited pronounced selectivity: stronger fluorine signals were detected in the eyespot (the highest) and chloroplasts, whereas almost no enrichment was observed in vacuoles or paramylon bodies within the exposure period. This specific distribution pattern suggests that environmentally relevant PFOS preferentially accumulates in the eyespot, chloroplasts, and mitochondria upon entering the cell. The high enrichment in the eyespot is particularly noteworthy, as the eyespot is located in the anterior plasma membrane region and may be more accessible to exogenous PFOS. Moreover, the carotenoid-protein complexes abundant in the eyespot may bind PFOS through hydrogen bonds and intermolecular forces[30], potentially disrupting the complex structure and interfering with phototransduction. Meanwhile, PFOS

accumulation in chloroplasts may disturb thylakoid membrane structure and electron transport chain function, while its presence in mitochondria may affect the tricarboxylic acid (TCA) cycle and oxidative phosphorylation.

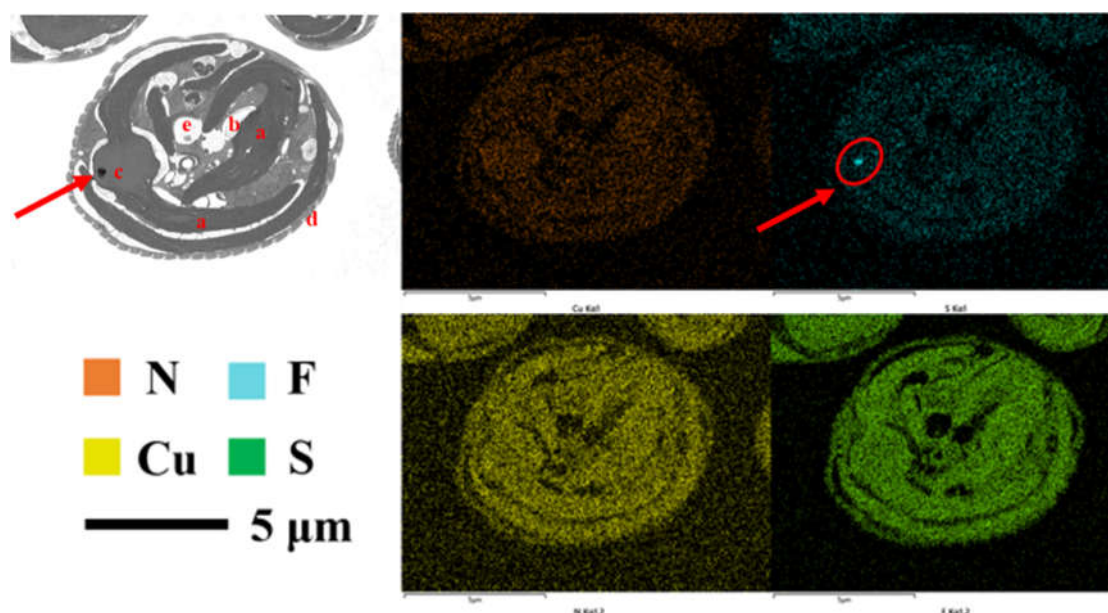


**Figure 1.** Subcellular distribution of PFOS in *E. gracilis* visualized by transmission electron microscopy (TEM) and corresponding TEM-energy-dispersive X-ray spectroscopy (EDS) mapping. TEM images of cell sections with major organelles labeled: chloroplast (a), paramylon body (b), eyespot (c), plasma membrane (d), and vacuole (e). The enhanced fluorine signals (indicative of PFOS accumulation) are observed in the eyespot.

To computationally assess whether PFOS can interact with the photoreceptor protein in the eyespot, the photoactivated adenylyl cyclase (PAC), which is involved in blue-light signal transduction, was selected as the docking target. As a high-resolution crystal structure of PAC is currently unavailable, a predicted structure was obtained by homology modeling to evaluate the binding potential of PFOS to the active pocket. The docking results (Figure 2) showed a predicted binding energy of  $-9.2$  kcal/mol between PFOS and PAC. The binding energy range for stable complex formation between PFOS and its core target proteins has been reported to be between  $-4.9$  and  $-9.7$  kcal/mol[31], indicating a strong affinity between PFOS and PAC. PFOS was localized within the active pocket and potentially formed hydrogen bonds, halogen bonds, or salt bridges with residues such as Arg126, Tyr204, and Trp98. Ishikawa et al. [32] previously reported that PFOS can undergo electrostatic interactions with basic amino acid residues of various proteins, which is consistent with our docking results.

Phototaxis assays further revealed changes in the phototactic behavior of *E. gracilis* after PFOS exposure (Figure 3a). At a low PFOS concentration ( $0.5$   $\mu\text{g/L}$ ), a unique “photosensitive biphasic effect” was observed: at low light intensities (2000–4000 lux), the sensitivity of cells to light was markedly enhanced; however, when the light intensity increased to 6000–10,000 lux, the phototactic response diminished, and the light saturation threshold decreased from 10,000 lux (control) to approximately 6000 lux. A possible explanation is that mild binding of PFOS to PAC at low concentrations lowers the trigger threshold for phototransduction, resulting in hypersensitivity under weak light. As light intensity increases, the impaired light-adaptation feedback mechanism fails to properly regulate signal gain, leading to premature light saturation[33]. At a high PFOS concentration ( $50.0$   $\mu\text{g/L}$ ), global phototaxis inhibition occurred, with the entire light-response curve shifted downward, indicating severe functional damage to the photoreceptive system.

Flagella are the executive organs of phototactic movement. The flagellar shedding rate increased in a concentration-dependent manner after PFOS exposure (Figure 3b): at low concentrations ( $0.5$ – $5.0$   $\mu\text{g/L}$ ), the shedding rate increased slightly but not significantly, whereas at  $50.0$   $\mu\text{g/L}$  it rose markedly

from 30% to 48.7%, and microscopic observation revealed evident flagellar shedding in PFOS-treated cells (Figure S2). This change directly impairs active cell motility. Swimming speed measurements (Figure 3c) were consistent with this pattern: both vertical and horizontal swimming speeds decreased with increasing PFOS concentration, with vertical movement being more severely affected. The increase in flagellar shedding may be related to PFOS-induced disruption of membrane lipid-protein interactions[34], and the reduced vertical swimming ability may further affect the vertical migration of cells in the water column and their access to light resources.

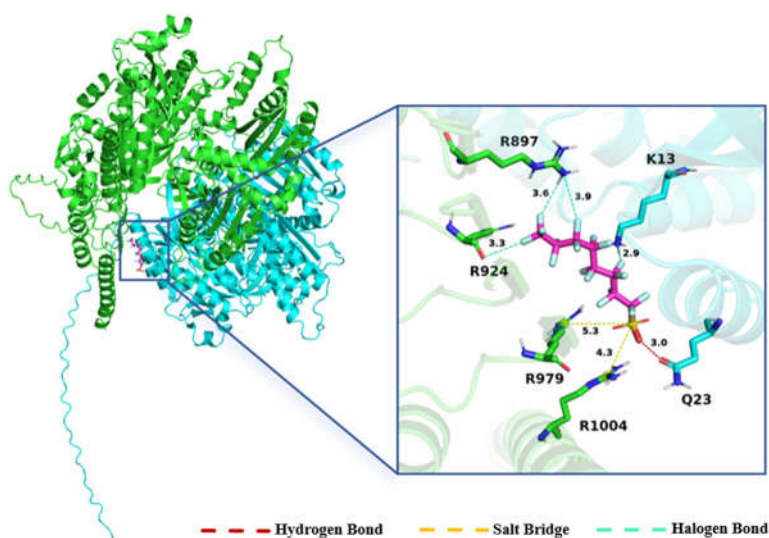


**Figure 2. Molecular docking of PFOS with PAC.** PFOS (pink stick, with wathet fluorine atoms) binds to the active pocket of PAC. Hydrogen \halogen bonds and salt bridges are indicated by dashed lines.

In summary, the eyespot accumulation and phototactic abnormalities observed in this section reflect a direct disturbance of the photoreceptive-motor system by PFOS. This disturbance impairs the ability of *E. gracilis* to actively approach or escape from specific light environments, thereby compromising the spatial positioning efficiency for light resource acquisition in the water column.

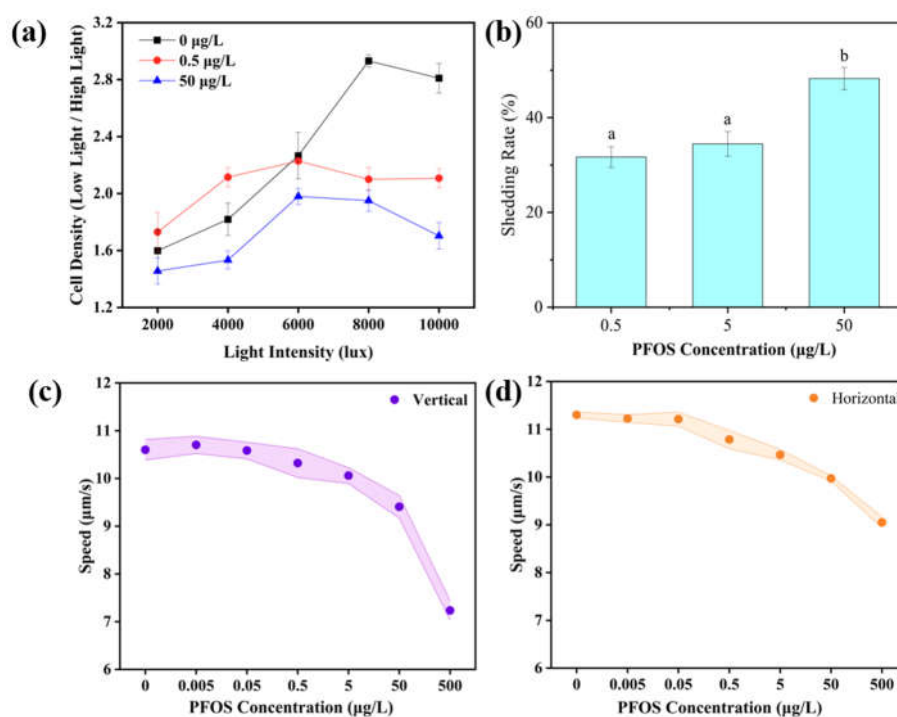


**Figure 3. Effects of PFOS exposure on phototaxis, flagellar shedding, and swimming speed of *E. gracilis*.** (a) Phototactic response (ratio of cell density at the near-light end to that at the far-light end) under different light intensity. (b) Flagellar shedding rate. (c) Vertical swimming speed. (d) Horizontal swimming speed. Different lowercase letters indicate significant differences among groups ( $p < 0.05$ ).

### 3.2. Changes in Photosynthetic Parameters and Their Decoupling from Energy Metabolism

Although PFOS accumulated markedly in the eyespot and impaired cell motility, overall photosynthesis was not suppressed in the short term; instead, a moderate enhancement was observed. *E. gracilis* contains chlorophyll a (Chl a), chlorophyll b (Chl b), carotenoids and other pigments (Cx+c). As shown in Figure S3, exposure to 0.5 and 50.0  $\mu\text{g/L}$  PFOS generally increased intracellular chlorophyll content, with Chl a being the most responsive. Compared with the control, 0.5  $\mu\text{g/L}$  PFOS significantly elevated Chl a content; Chl b and other pigments also increased, though not significantly. At 50.0  $\mu\text{g/L}$  PFOS, chlorophyll content still tended to be higher than the control, but the difference did not reach statistical significance. Overall, environmentally relevant PFOS caused a slight stimulation of chlorophyll content, which is more likely a short-term stress response rather than a genuine improvement in photosynthetic capacity. Similar inductions of photosynthetic pigments have been reported under other pollutant stresses[35] and are generally interpreted as a compensatory strategy when light capture efficiency is threatened.

Non-photochemical quenching (NPQ) is a key photoprotective mechanism that dissipates excess excitation energy as heat, whereas  $Fv/Fm$  reflects the maximum photochemical efficiency of photosystem II (PSII). Under normal conditions, increased NPQ indicates enhanced photoprotection, and decreased  $Fv/Fm$  signifies damage to PSII reaction centers. Previous studies have shown that high PFOS concentrations damage microalgal photosynthesis, while lower concentrations may cause transient stimulation[36]. In this study, exposure to 0.5–50.0  $\mu\text{g/L}$  PFOS led to significant increases in  $Fv/Fm$  at several time points, particularly on day 3, and the elevation became even more pronounced by day 7 (Figure 4a). NPQ also increased significantly on days 2 and 7 (Figure 4b). The temporal patterns of  $Fv/Fm$  and NPQ were generally consistent, suggesting that PFOS triggered a photoprotective regulatory response. Li et al.[37] also observed a short-term stimulation of photosynthetic activity in *Chlamydomonas reinhardtii* by low-concentration PFOS, which they attributed to stress-induced upregulation of PSII reaction center activity. Nevertheless, such upregulation should be viewed as an adaptive stress response rather than evidence of true photosynthetic improvement.

Importantly, the simultaneous increases in chlorophyll content,  $Fv/Fm$ , and NPQ are not readily reconciled with the expectation that eyespot damage would reduce light capture capacity. In other words, although PFOS accumulated in the eyespot and impaired phototaxis, the *in vivo* photosynthetic system did not show a corresponding downregulation; instead, it displayed signs of upregulation. This discrepancy suggests that eyespot dysfunction does not directly translate into a measurable loss of light capture efficiency under the present experimental conditions, and the observed changes in photosynthetic parameters are more likely attributable to direct effects of PFOS on chloroplasts.

Does this short-term upregulation of photosynthetic parameters confer a real growth advantage? Growth curve monitoring (Figure 4c) revealed that low PFOS concentrations (0.5–5.0  $\mu\text{g/L}$ ) promoted growth on days 7–10, with the 0.5  $\mu\text{g/L}$  group showing the strongest effect. The 50.0  $\mu\text{g/L}$  group also exhibited a weak promotion on days 7–8, but by day 10, it began to show an inhibitory trend, with cell density falling below that of the control. Thus, the effect of PFOS on growth is not a simple linear inhibition. At early time points and lower concentrations, cells may obtain a transient growth stimulus via compensatory mechanisms; however, as exposure time and concentration increase, toxicity accumulates and eventually dominates. This low-concentration stimulation/high-concentration inhibition pattern is known as hormesis[38], which typically reflects a dynamic balance between the activation and exhaustion of cellular defense systems.

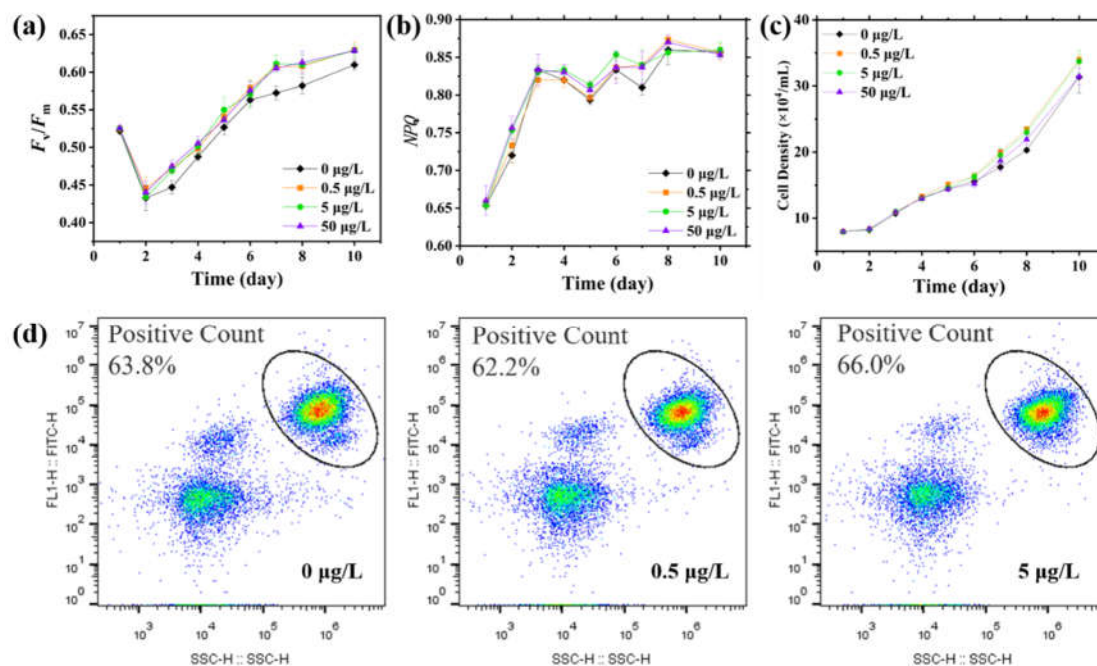


**Figure 4.** Effects of PFOS exposure on photosynthetic parameters, growth, and ROS levels in *E. gracilis*. (a) Maximum photochemical efficiency of PSII ( $F_v/F_m$ ). (b) Non-photochemical quenching (NPQ). (c) Growth curves (cell density over 10 days). (d) Intracellular reactive oxygen species (ROS) levels (percentage of cells with high ROS positivity).

Nevertheless, the weak growth promotion did not translate into improved cellular energy status. Further analysis showed that intracellular ATP levels decreased progressively with increasing PFOS concentration (Figure 5). Compared with the control, ATP content in all treatment groups was significantly reduced in a concentration-dependent manner. Hence, although some photosynthetic parameters were upregulated, energy metabolism did not improve; on the contrary, energy output appeared constrained. This indicates that the primary impact of PFOS on *E. gracilis* may not be on light capture per se, but rather on downstream energy conversion processes. Measurements of reactive oxygen species (ROS) provide supporting evidence. PFOS exposure elevated intracellular ROS levels (Figure 4d). Relative to the control, the proportion of cells with high ROS positivity decreased slightly from 63.8% to 62.2% at 0.5  $\mu\text{g/L}$  PFOS but increased to 66% at 5.0  $\mu\text{g/L}$  PFOS. This pattern is consistent with a hormetic response: at low concentrations, the antioxidant defense system may be moderately activated, preventing a rise in ROS; at higher concentrations, oxidative stress overwhelms the scavenging capacity, leading to ROS accumulation. Elevated ROS can directly damage photosynthetic membrane lipids and protein complexes and also consume cellular reducing equivalents, further burdening the electron transport chain.

Taken together, the in vivo data in this section reveal a coherent yet paradoxical picture: after PFOS exposure, photosynthetic parameters (chlorophyll,  $F_v/F_m$ , NPQ) and growth show transient upregulation, but ATP output continuously declines, and ROS levels display a concentration-dependent biphasic pattern. This decoupling between the photosynthetic phenotype and energy metabolism – especially the divergence between elevated  $F_v/F_m$  and reduced ATP – strongly suggests that direct interference of PFOS with chloroplast energy conversion (rather than an initial defect in light capture) is the key to understanding these seemingly contradictory observations.

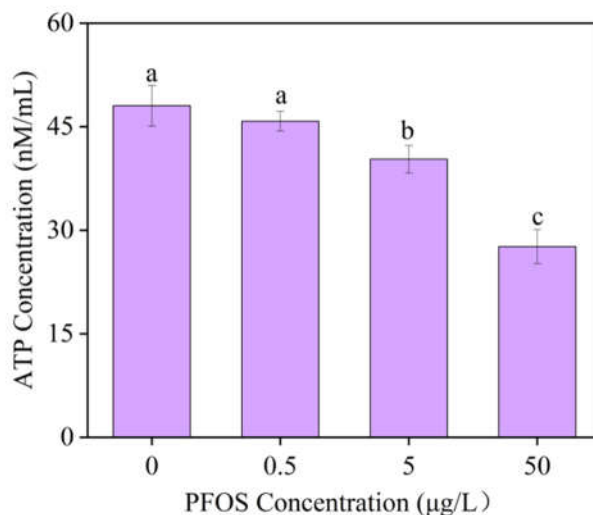


**Figure 5. Intracellular ATP levels in *E. gracilis* exposed to different concentrations of PFOS (0, 0.5, 5.0, and 50.0 µg/L).** Data are presented as mean  $\pm$  SD ( $n = 3$ ). Different lowercase letters indicate significant differences among groups ( $p < 0.05$ ).

### 3.3. Isolated Chloroplast Assays Reveal Direct Inhibition of $Mg^{2+}$ -ATP Synthase and Secondary Impairment of Electron Transport by PFOS

The *in vivo* observations of “enhanced light capture but decreased ATP output” together with increased ROS levels suggested that PFOS may affect the photosynthetic system of *E. gracilis* through two possible pathways: (i) indirect effects via accumulation in the eyespot and flagella, which might disturb whole-cell physiology, and (ii) direct actions on chloroplasts, such as inhibition of ATP synthase or interference with the electron transport chain. To distinguish between these possibilities, isolated chloroplasts from autotrophically grown *E. gracilis* were exposed to PFOS concentrations (0–500 ng/L) that mimic subcellular accumulation levels.

The effect of PFOS on the photosynthetic electron transport rate (*ETR*) of isolated chloroplasts was concentration-dependent. No significant change in *ETR* was observed at 5.0 ng/L PFOS, whereas *ETR* decreased significantly at 50.0 and 500.0 ng/L ( $p < 0.05$ ; Figure 6a). *ETR* reflects the overall operation of the photosynthetic electron transport chain. However, as detailed below, this decline in *ETR* is likely secondary to the inhibition of ATP synthase and the consequent accumulation of the thylakoid proton gradient ( $\Delta pH$ ), which triggers feedback inhibition of electron transport, rather than a direct action of PFOS on the electron transport chain itself.

To identify potential direct targets of PFOS within the electron transport chain, the activity of the cytochrome *b6f* (*Cyt b6f*) complex was measured. *Cyt b6f* is a critical electron transfer node between photosystem II (PSII) and photosystem I (PSI). As shown in Figure 6b, *Cyt b6f* activity increased slightly but not significantly at 5.0 ng/L PFOS, then gradually decreased at 50.0 and 500.0 ng/L, with significant inhibition observed only at 500.0 ng/L. Comparing the responses of *ETR* and *Cyt b6f* revealed that *ETR* was much more sensitive to PFOS than *Cyt b6f*. At 50.0 ng/L, *Cyt b6f* decreased only mildly, whereas *ETR* was already significantly inhibited. This discrepancy suggests that the suppression of electron transport is unlikely to be explained solely by direct inhibition of a single complex such as *Cyt b6f*. Instead, it is consistent with a feedback inhibition mechanism triggered by  $\Delta pH$  accumulation resulting from ATP synthase inhibition, which would broadly suppress electron flow downstream of PSII.

Impairment of the electron transport chain inevitably affects the establishment of the trans-thylakoid proton gradient, which is the direct driving force for ADP phosphorylation by ATP synthase[39]. Measurements of photophosphorylation activity (Figure 6c–e) confirmed that ATP synthase is a primary target. At 5.0 ng/L PFOS, photophosphorylation activity increased slightly but

not significantly; at 50.0 ng/L, activity decreased significantly ( $p < 0.05$ ); and at 500.0 ng/L, the decrease was even more pronounced ( $p < 0.01$ ). The change in  $Mg^{2+}$ -ATPase activity followed a pattern similar to that of photophosphorylation, whereas  $Ca^{2+}$ -ATPase activity did not change significantly in any treatment group. This ion-dependent selectivity indicates that  $Mg^{2+}$ -ATP synthase is a sensitive target of PFOS. Siedlecka et al.[40] reported that certain organic pollutants can selectively inhibit  $Mg^{2+}$ -ATPase while sparing  $Ca^{2+}$ -ATPase activity, which is consistent with our findings.

To further investigate the impact of PFOS on the electrochemical properties of chloroplasts, electrochemical impedance spectroscopy (EIS) and cyclic voltammetry (CV) were performed on isolated chloroplasts (Figure 6f). EIS results showed that the membrane/interface resistance in the equivalent circuit of chloroplasts first decreased and then increased with increasing PFOS concentration. At low concentration, a mild change in membrane fluidity might reduce ion transmembrane resistance; at high concentration, the interface membrane resistance increased significantly. This change likely does not arise from simple physical membrane damage but rather from multiple functional disturbances at the molecular level. The decline in ATP synthase activity leads to ATP shortage, which in turn impairs ATP-dependent transmembrane ion pumps (e.g.,  $H^+$ -ATPase,  $Ca^{2+}$ -ATPase), further aggravating ion transport disturbance. This may be an important contributing factor to the increased membrane interface resistance. The CV curves showed that at 5.0 ng/L PFOS, both the oxidation and reduction peaks of chloroplasts were slightly enhanced, indicating that low-concentration PFOS might exert a mild stimulatory effect on the chloroplast membrane system, resulting in a transient increase in electrochemical response. At higher concentrations (50.0 and 500.0 ng/L), the oxidation and reduction peaks gradually weakened, suggesting that higher PFOS concentrations inhibit thylakoid membrane structure and electron transfer processes.

The key finding of the isolated chloroplast assays is that, even in the complete absence of whole-cell regulatory factors, PFOS directly inhibits  $Mg^{2+}$ -ATP synthase activity, leading to a secondary impairment of electron transport efficiency and altered electrochemical characteristics of thylakoid membranes. This indicates that the action of PFOS on the photosynthetic apparatus has a degree of chloroplast autonomy and does not depend on eyespot signaling or nuclear regulation. The observed decrease in *ETR* is therefore a consequence of feedback inhibition driven by  $\Delta pH$  accumulation, rather than a direct block of the electron transport chain.

#### 3.4. Integrative Transcriptomic and Proteomic Analyses Reveal Compensatory Responses and Energy Metabolism Imbalance Induced by PFOS

The isolated chloroplast assays demonstrated that PFOS directly inhibits  $Mg^{2+}$ -ATP synthase activity, reduces photophosphorylation efficiency, and interferes with thylakoid membrane electron transport. To further elucidate the molecular underpinnings, transcriptomic and proteomic analyses were performed on *E. gracilis* exposed to 50.0  $\mu g/L$  PFOS for 7 days.

Transcriptome analysis identified 252 significantly differentially expressed genes, of which 230 were downregulated and only 22 were upregulated, indicating that prolonged PFOS exposure leads to a predominantly suppressive transcriptional regulation. GO enrichment analysis (Figure 7a–b) showed that the differentially expressed genes were mainly involved in oxidoreductase activity, lipid metabolism, carbohydrate metabolism, and catalytic activity. KEGG enrichment analysis (Figure 7c–d) further revealed that PFOS affects amino acid metabolism, lipid metabolism, photosynthesis, chlorophyll metabolism, the TCA cycle, and the phosphatidylinositol signaling pathway. Notably, the upregulation of genes related to photosynthesis and chlorophyll metabolism is consistent with the increased chlorophyll content (Figure S3) and elevated *Fv/Fm* (Figure 4a) observed physiologically, suggesting that cells initiate a compensatory response at the transcriptional level to enhance light capture, rather than indicating a genuinely efficient photosynthetic state.

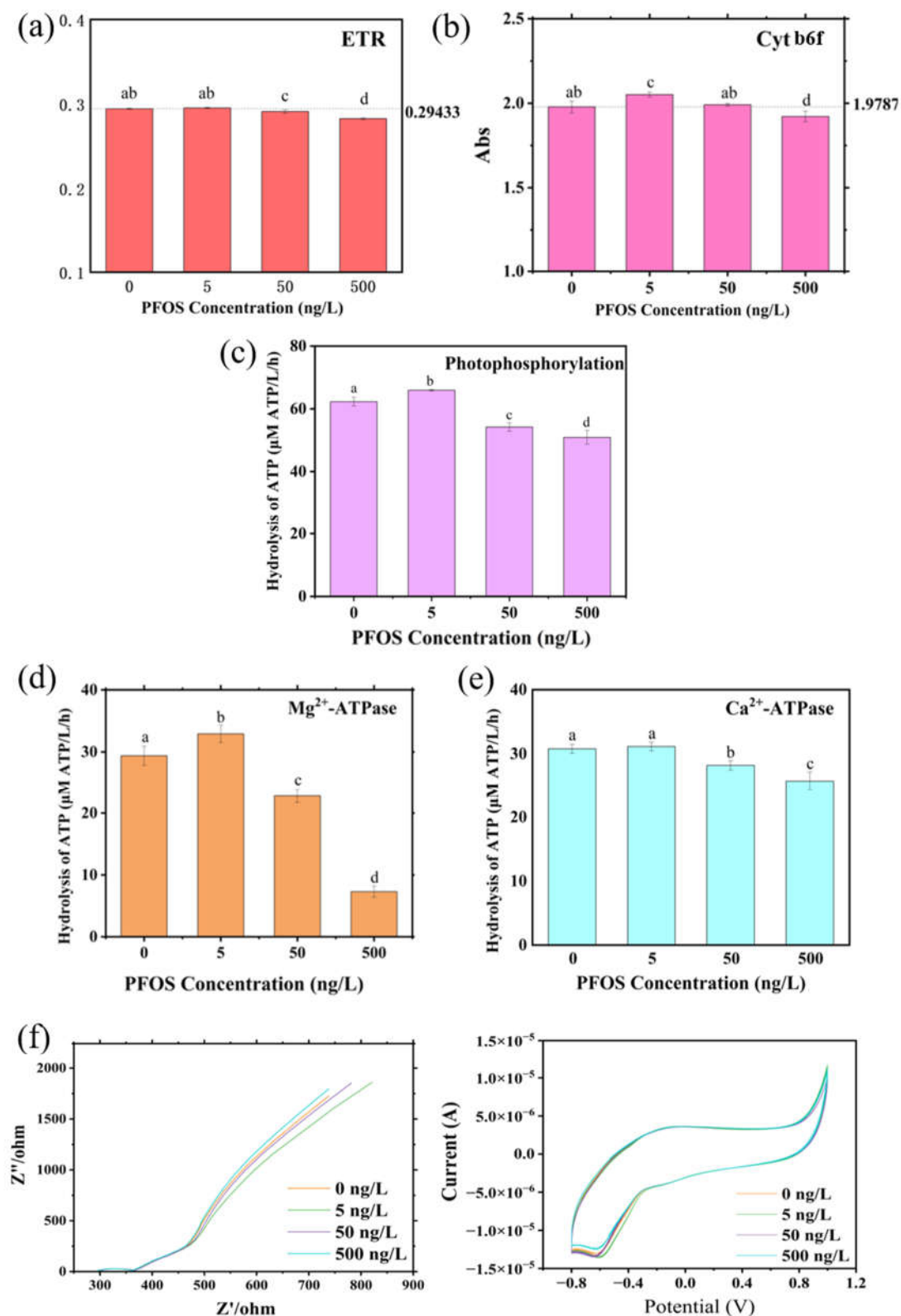


**Figure 6.** Effects of PFOS on isolated chloroplasts of *E. gracilis*. (a) Cytochrome b6/f complex activity. (b) Photosynthetic electron transport rate (ETR). (c) Photophosphorylation activity. (d)  $\text{Mg}^{2+}$ -ATPase activity. (e)  $\text{Ca}^{2+}$ -ATPase activity. (f) Electrochemical impedance spectroscopy (EIS) Nyquist plots and cyclic voltammetry (CV) curves. Chloroplasts were exposed to PFOS at 0, 5.0, 50.0, and 500.0 ng/L. Data in (a–e) are presented as mean  $\pm$  SD ( $n = 3$ ). Different lowercase letters indicate significant differences among groups ( $p < 0.05$ ).

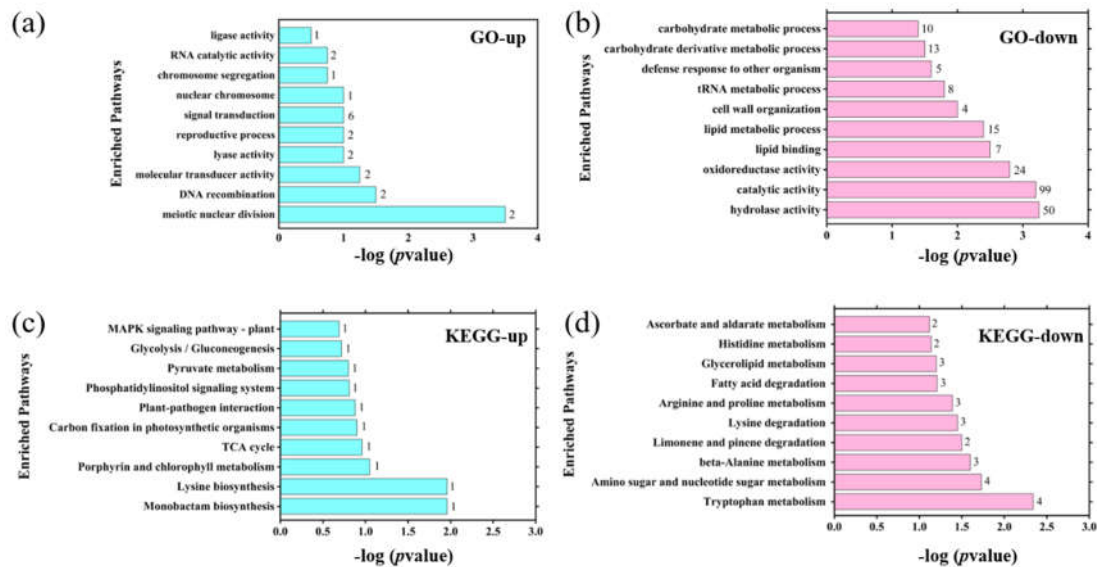


**Figure 7.** GO and KEGG enrichment analyses of differentially expressed genes in *E. gracilis* exposed to 50.0  $\mu\text{g/L}$  PFOS for 7 days. (a) GO enrichment of upregulated genes. (b) GO enrichment of downregulated genes. (c) KEGG enrichment of upregulated genes. (d) KEGG enrichment of downregulated genes. The numbers in the bars correspond to the number of genes enriched in each pathway (for a and c: number of upregulated genes; for b and d: number of downregulated genes). Only significantly enriched terms ( $p < 0.05$ ) are shown.

The proteomic data provided more direct molecular evidence. Subcellular localization analysis of differentially expressed proteins (Figure 8) showed that the chloroplast was the most significantly affected compartment, in excellent agreement with the isolated chloroplast assays. GO enrichment analysis (Figure 9) revealed that upregulated proteins were mainly enriched in chloroplast function, lipid metabolism, and magnesium ion binding, whereas downregulated proteins were significantly enriched in ATP synthesis, peroxidase activity, and zinc/transition metal ion binding. Among these, the downregulation of ATP synthesis-related proteins directly corroborates the decreased  $\text{Mg}^{2+}$ -ATP synthase activity observed in isolated chloroplasts (Figure 6d) and is consistent with the reduced intracellular ATP levels (Figure 5). This reveals a molecular imbalance characterized by “upstream enhancement but downstream blockage”: although genes involved in light capture and chlorophyll metabolism are upregulated, the terminal step of energy conversion—ATP synthase function—is impaired, leading to a decoupling between light capture and energy utilization. Previous studies have shown that when ATP synthase function is compromised, photosynthetic organisms upregulate the expression of light-harvesting complexes via feedback mechanisms[41]; however, such compensation cannot restore the loss of energy conversion efficiency. KEGG pathway enrichment analysis of the proteomic data (Figure S4) further revealed that proteins involved in photosynthetic processes were increased, whereas those related to carotenoid biosynthesis were decreased. The upregulation of photosynthetic proteins is consistent with the increased chlorophyll content (Figure S3) and elevated *Fv/Fm* (Figure 4a), reinforcing the view that cells mount a compensatory response to enhance light capture. In contrast, the downregulation of carotenoid biosynthesis may affect eyespot function (as the eyespot is rich in carotenoids) and photoprotection, although *NPQ* was elevated (Figure 4b).



thylakoid membranes, indicating that PFOS acts at multiple levels, affecting both membrane systems and energy metabolism.

Taken together, the results form a self-consistent explanatory framework. PFOS accumulates in the *Euglena* eyespot, causing phototactic abnormalities and impaired motility—a direct disturbance of the photoreceptive-motor system. In vivo photosynthetic parameters did not decline with eyespot damage; instead, chlorophyll content,  $Fv/Fm$ , and  $NPQ$  increased, indicating that changes in the photosynthetic system cannot be attributed to eyespot impairment. Isolated chloroplast assays demonstrated that PFOS directly inhibits electron transport efficiency and  $Mg^{2+}$ -ATP synthase activity at the chloroplast level. Transcriptomic and proteomic results further revealed that *E. gracilis* initiates a compensatory response characterized by upregulation of photosynthesis-related processes under PFOS stress, but the downregulation of ATP synthesis-related proteins prevents recovery of energy conversion efficiency, resulting in a decoupled state of “upstream enhancement and downstream blockage”.

#### 4. Conclusions

In this study, we systematically investigated the effects of environmentally relevant concentrations of PFOS on phototaxis, photosynthetic function, and energy metabolism in the photoautotrophic flagellate *E. gracilis*.

(i) TEM-EDS mapping revealed that PFOS exhibited pronounced subcellular accumulation, with the highest fluorine signal enrichment in the eyespot, followed by chloroplasts and mitochondria. PFOS exposure induced a biphasic phototactic response at low concentrations (hypersensitivity at low light intensities but premature saturation at high light intensities) and global inhibition at high concentrations, accompanied by increased flagellar shedding and reduced swimming speed. These results indicate a clear disturbance of the photoreceptive and motor systems.

(ii) In vivo physiological data showed that environmentally relevant PFOS did not acutely inhibit the photosynthetic apparatus; instead, chlorophyll content,  $Fv/Fm$ , and  $NPQ$  were elevated, suggesting the activation of a compensatory photoprotective response. However, intracellular ATP levels progressively declined with increasing PFOS concentration, while ROS levels showed a concentration-dependent biphasic pattern (a slight decrease at low concentration and a marked increase at high concentration). Growth curves displayed a weak promotion at low concentrations and an inhibitory trend only at the highest concentration (50.0  $\mu\text{g/L}$ ) by day 10. The divergence between enhanced photochemical parameters and reduced ATP output indicates that the PFOS-induced upregulation of photosynthetic components is a stress-related compensation rather than a genuine functional improvement.

(iii) Isolated chloroplast assays demonstrated that PFOS directly inhibits  $Mg^{2+}$ -ATP synthase activity and leads to a secondary impairment of electron transport efficiency, accompanied by altered electrochemical characteristics of thylakoid membranes. Thus, the action of PFOS on the photosynthetic apparatus exhibits a degree of chloroplast autonomy. Integrative transcriptomic and proteomic analyses further revealed a molecular pattern characterized by upregulation of photosynthesis- and chlorophyll metabolism-related genes/proteins, alongside downregulation of ATP synthesis-related proteins and certain metal ion-binding proteins. This pattern reflects a compensatory response of “upstream enhancement but downstream blockage”.

Collectively, PFOS disrupts light resource utilization in *E. gracilis* by impairing both phototactic behavior and photophosphorylation. At the behavioral level, PFOS accumulates in the eyespot, interferes with phototaxis and motility, and thereby compromises the ability of cells to actively locate optimal light environments. At the physiological level, PFOS directly targets chloroplast  $Mg^{2+}$ -ATP synthase, suppresses photophosphorylation, and reduces ATP output. In response to the perceived energy deficit, cells mount a compensatory upregulation of photosynthetic processes, but this compensation cannot overcome the bottleneck imposed by impaired ATP synthase, ultimately leading to a decoupled state of “upstream enhancement and downstream blockage” and a significant reduction in the effective utilization of light resources.

This study provides new insights into the composite toxicity of PFOS to photosynthetic eukaryotic microorganisms, demonstrating that environmentally relevant PFOS can affect light resource utilization and energy homeostasis in *Euglena* through dual interference at the behavioral and physiological levels. These findings contribute to the risk assessment of PFAS in aquatic ecosystems.

**Supplementary Materials:** The following supporting information can be downloaded at the website of this paper posted on Preprints.org.

**Acknowledgments:** This work was supported by the National Natural Science Foundation of China (No. 42207517), and Zhejiang Key Laboratory of Low-carbon Control Technology for Industrial Pollution, Zhejiang University of Technology, (Grant No.2025DTZL02), (2025ZY01076).

**Declaration of competing interest:** The authors declare no competing financial interest.

## References

1. Ge, X.F.; Wang, K.; Xiao, X.; Chu, C.H.; Zhu, X.Y.; Chen, B.L. Beyond molecules: In situ imaging unveils dom-driven pfas nanoclusters with mitigated phytotoxicity. *Environmental Science & Technology* **2026**, *60*, 7393-7404.
2. Liao, J.; Sun, B.; Wang, C.; Cao, Z.; Wu, Z.; An, X.; Liang, Z.a.; Huang, X.; Lu, Y. Uptake and cellular responses of microcystis aeruginosa to pfos in various environmental conditions. *Ecotoxicology and Environmental Safety* **2024**.
3. Xu, C.; Xu, C.; Zhou, Q.; Shen, C.; Peng, L.; Liu, S.; Yin, S.; Li, F. Spatial distribution, isomer signature and air-soil exchange of legacy and emerging poly- and perfluoroalkyl substances. *Environmental Pollution* **2024**, *343*, 123222.
4. Chen, Y.; Wei, L.J.; Luo, W.; Jiang, N.; Shi, Y.L.; Zhao, P.; Ga, B.L.; Pei, Z.G.; Li, Y.M.; Yang, R.Q., et al. Occurrence, spatial distribution, and sources of pfas in the water and sediment from lakes in the tibetan plateau. *Journal of Hazardous Materials* **2023**, *443*, 130170.
5. Liao, J.M.; Sun, B.; Wang, C.; Cao, Z.W.; Wu, Z.Y.; An, X.P.; Liang, Z.A.; Huang, X., Y.; Lu, Y.L. Uptake and cellular responses of *microcystis aeruginosa* to pfos in various environmental conditions. *Ecotoxicology and Environmental Safety* **2024**, *272*, 116041.
6. Li, W.Z.; Li, H.Z.; Zhang, D.N.; Tong, Y.J.; Li, F.X.; Cheng, F.; Huang, Z.B.; You, J. Legacy and emerging per- and polyfluoroalkyl substances behave distinctly in spatial distribution and multimedia partitioning: A case study in the pearl river, china. *Environmental Science & Technology* **2022**, *56*, 3492-3502.
7. Meng, L.Y.; Song, B.Y.; Zhong, H.F.; Ma, X.D.; Wang, Y.J.; Ma, D.H.; Lu, Y.; Gao, W.; Wang, Y.W.; Jiang, G.B. Legacy and emerging per- and polyfluoroalkyl substances (pfas) in the bohai sea and its inflow rivers. *Environment International* **2021**, *156*, 106735.
8. Xiao, S.K.; Wu, Q.; Pan, C.G.; Yin, C.; Wang, Y.H.; Yu, K.F. Distribution, partitioning behavior and potential source of legacy and alternative per- and polyfluoroalkyl substances (pfas) in water and sediments from a subtropical gulf, south china sea. *Environmental Research* **2021**, *201*, 111485.
9. Jones, P.D.; Hu, W.; De Coen, W.; Newsted, J.L.; Giesy, J.P. Binding of perfluorinated fatty acids to serum proteins. *Environmental Toxicology and Chemistry* **2003**.
10. Iseki, M.; Matsunaga, S.; Murakami, A.; Ohno, K.; Shiga, K.; Yoshida, K.; Sugai, M.; Takahashi, T.; Hori, T.; Watanabe, M. A blue-light-activated adenylyl cyclase mediates photoavoidance in *euglena gracilis*. *Nature* **2002**.
11. Zhu, J.; Tan, X.; Hafid, H.S.; Wakisaka, M. Enhancement of biomass yield and lipid accumulation of freshwater microalga *euglena gracilis* by phenolic compounds from basic structures of lignin. *Bioresource Technology* **2020**.
12. Häder, D.-P.; Lebert, M. Photoorientation in photosynthetic flagellates. *Methods in Molecular Biology* **2009**.
13. Xu, D.; Chen, X.; Shao, B. Oxidative damage and cytotoxicity of perfluorooctane sulfonate on *chlorella vulgaris*. *Bulletin of Environmental Contamination and Toxicology* **2016**.

14. Poothong, S.; Boontanon, S.K.; Boontanon, N. Determination of perfluorooctane sulfonate and perfluorooctanoic acid in food packaging using liquid chromatography coupled with tandem mass spectrometry. *Journal of Hazardous Materials* **2012**.
15. Kanna, S.D.; Domonkos, I.; Kobori, T.O.; Dergez, A.; Bode, K.; Nagyapati, S.; Zsiros, O.; Unnep, R.; Nagy, G.; Garab, G., et al. Salt stress induces paramylon accumulation and fine-tuning of the macro-organization of thylakoid membranes in *euglena gracilis* cells. *Frontiers in Plant Science* **2021**, *12*, 725699.
16. Liu, Y.; Yang, X.; Gan, J.; Chen, S.; Xiao, Z.-X.; Cao, Y. Cb-dock2: Improved protein-ligand blind docking by integrating cavity detection, docking and homologous template fitting. *Nucleic Acids Research* **2022**.
17. Wang, Y.; Fan, X.; Gao, G.; Beardall, J.; Inaba, K.; Hall-Spencer, J.M.; Xu, D.; Zhang, X.; Han, W.; McMinn, A., et al. Decreased motility of flagellated microalgae long-term acclimated to CO<sub>2</sub>-induced acidified waters. *Nature Climate Change* **2020**, *10*, 561-567.
18. Zhu, J.; Tan, X.; Hafid, H.S.; Wakisaka, M. Enhancement of biomass yield and lipid accumulation of freshwater microalga *euglena gracilis* by phenolic compounds from basic structures of lignin. *Bioresource Technology* **2021**, 321.
19. Kim, H.; Van Duong, H.; Kim, E.; Lee, B.G.; Han, S. Effects of phytoplankton cell size and chloride concentration on the bioaccumulation of methylmercury in marine phytoplankton. *Environmental Toxicology* **2014**, *29*, 936-941.
20. Zheng, S.; Zhang, C.; Shi, K.; Wang, J.; Sun, G.; Hu, Q.; Zhao, F.; Wang, X. Bioaccumulation, subcellular distribution and chemical forms of yttrium in rice seedling. *Journal of Rare Earths* **2018**, *36*, 331-336.
21. Cara, B.; Lies, T.; Thimo, G.; Robin, L.; Lieven, B. Bioaccumulation and trophic transfer of perfluorinated alkyl substances (PFAS) in marine biota from the Belgian North Sea: Distribution and human health risk implications. *Environmental Pollution* **2022**, *311*, 119907.
22. Li, J.; Sun, J.; Li, P. Exposure routes, bioaccumulation and toxic effects of per- and polyfluoroalkyl substances (PFAS) on plants: A critical review. *Environment International* **2022**, *158*, 106891.
23. Heyno, E.; Ermakova, M.; Lopez-Calcagno, P.E.; Woodford, R.; Brown, K.L.; Matthews, J.S.A.; Osmond, B.; Raines, C.A.; von Caemmerer, S. Rieske Fe overexpression in tobacco provides increased abundance and activity of cytochrome b<sub>6</sub>/f. *Physiol Plant* **2022**, *174*, e13803.
24. U DWIVEDI, R.B., M SHARMA. Alteration in the acceptor side of photosystem II of chloroplast by high light. *Journal of Biosciences* **1996**, *21*, 527-533.
25. Richter, L.V.; Mansfeldt, C.B.; Kuan, M.M.; Cesare, A.E.; Menefee, S.T.; Richardson, R.E.; Ahner, B.A. Altered microbiome leads to significant phenotypic and transcriptomic differences in a lipid accumulating chlorophyte. *Environmental Science & Technology* **2018**, *52*, 6854-6863.
26. Gschloessl, B.; Dorkeld, F.; Berges, H.; Beydon, G.; Bouchez, O.; Branco, M.; Bretaudeau, A.; Burban, C.; Dubois, E.; Gauthier, P., et al. Draft genome and reference transcriptomic resources for the urticating pine defoliator *thaumetopoea pityocampa* (Lepidoptera: Notodontidae). *Mol Ecol Resour* **2018**, *18*, 602-619.
27. Zhao, Y.; Zhang, Z.; Li, M.; Luo, J.; Chen, F.; Gong, Y.; Li, Y.; Wei, Y.; Su, Y.; Kong, L. Transcriptomic profiles of 33 opium poppy samples in different tissues, growth phases, and cultivars. *Scientific Data* **2019**, *6*, 66.
28. Muntel, J.; Xuan, Y.; Berger, S.T.; Reiter, L.; Bachur, R.; Kentsis, A.; Steen, H. Advancing urinary protein biomarker discovery by data-independent acquisition on a quadrupole-orbitrap mass spectrometer. *Journal of Proteome Research* **2015**, *14*, 4752-4762.
29. Chiva, C.; Mendes Maia, T.; Panse, C.; Stejskal, K.; Douche, T.; Matondo, M.; Loew, D.; Helm, D.; Rettel, M.; Mechtler, K., et al. Quality standards in proteomics research facilities: Common standards and quality procedures are essential for proteomics facilities and their users. *Science & Society* **2021**, *22*, e52626.
30. Bischel, H.N.; MacManus-Spencer, L.A.; Luthy, R.G. Noncovalent interactions of long-chain perfluoroalkyl acids with serum albumin. *Environmental Science & Technology* **2010**.
31. Mao, W.; Li, M.; Xue, X.; Cao, W.; Wang, X.; Xu, F.; Jiang, W. Bioaccumulation and toxicity of perfluorooctanoic acid and perfluorooctane sulfonate in marine algae *Chlorella* sp. *Science of the Total Environment* **2023**.
32. Jahanban-Esfahlan, A.; Ostadrahimi, A.; Jahanban-Esfahlan, R.; Roufegarinejad, L.; Tabibiazar, M.; Amarowicz, R. Recent developments in the detection of bovine serum albumin. *International Journal of Biological Macromolecules* **2019**.

33. Ozasa, K.; Won, J.; Song, S.; Shinomura, T.; Maeda, M. Phototaxis and photo-shock responses of euglena gracilis under gravitaxis. *Algal Research* **2019**.
34. Hu, W.y.; Jones, P.D.; DeCoen, W.; King, L.; Fraker, P.; Newsted, J.; Giesy, J.P. Alterations in cell membrane properties caused by perfluorinated compounds. *Comparative Biochemistry and Physiology C: Toxicology & Pharmacology* **2003**.
35. Scheuerlein, R.; Treml, S.; Thar, B.; Tirlapur, U.K.; Häder, D.-P. Evidence for uv-b-induced DNA degradation in euglena gracilis mediated by activation of metal-dependent nucleases. *Journal of Photochemistry and Photobiology B: Biology* **1995**.
36. Davis, S.N.; Klumker, S.M.; Mitchell, A.A.; Coppage, M.A.; Labonté, J.M.; Quigg, A. Life in the pfas lane: The impact of perfluoroalkyl substances on photosynthesis, cellular exudates, nutrient cycling, and composition of a marine microbial community. *Science of the Total Environment* **2024**.
37. Homburg, S.V.; Kruse, O.; Patel, A.V. Growth and photosynthetic activity of chlamydomonas reinhardtii entrapped in lens-shaped silica hydrogels. *Journal of Biotechnology* **2019**.
38. Calabrese, E.J.; Baldwin, L.A. Hormesis: The dose-response revolution. *Annual Review of Pharmacology and Toxicology* **2002**.
39. Mitchell, P. Coupling of phosphorylation to electron and hydrogen transfer by a chemi-osmotic type of mechanism. *Nature* **1961**.
40. Heidarian, F.; Fallah, S.; Pokhrel, L.R.; Rostamnejadi, A. Magnetite nanoparticles (Fe<sub>3</sub>O<sub>4</sub>NPs) promote drought tolerance and improve plant health, grain quality and yield in kidney bean (phaseolus vulgaris l.). *Science of the Total Environment* **2025**.
41. Johnson, M.P. Structure, regulation and assembly of the photosynthetic electron transport chain. *Nature Reviews Molecular Cell Biology* **2025**.

**Disclaimer/Publisher's Note:** The statements, opinions and data contained in all publications are solely those of the individual author(s) and contributor(s) and not of MDPI and/or the editor(s). MDPI and/or the editor(s) disclaim responsibility for any injury to people or property resulting from any ideas, methods, instructions or products referred to in the content.